Communication

Recovery of Ni-Co-Mn Oxides from End-of-Life Lithium-Ion Batteries for the Application of a Negative Temperature Coefficient Sensor

Sungwook Mhin

Department of Advanced Materials Engineering, Kyonggi University, Suwon 16227, Republic of Korea; swmhin@kgu.ac.kr

Abstract: This study demonstrates the current advancements in battery management systems (BMSs), emphasizing the need for precise temperature monitoring within battery packs to enhance safety and performance through efficient thermal management. The increased demand for lithium-ion batteries (LIBs) has driven the development of temperature sensors with improved accuracy and stability. In particular, Ni-Co-Mn-based spinel oxides are commonly used due to their stable negative temperature coefficient (NTC) behavior. However, challenges arise in manufacturing due to the high cost and uncertain supply of critical cathode components (e.g., Co, Ni, and Mn) for LIBs. This research focuses on developing spinel-type $(Ni_{0.6}Co_{0.4}Mn_2)O_4$ using recycled Ni-Co-Mn oxides obtained from end-of-life (EOL) LIBs, demonstrating temperature resistance behavior suitable for temperature sensing. The oxides are prepared through hydrometallurgy, oxalate synthesis, and post-heat treatment. Successful integration into spinel-type NTC thermistors suggests broader applications in various industrial fields. A systematic investigation into the synthesis and characterization of recovered Ni-Co-Mn oxides from EOL LIB cathode materials $(Li(Ni_{0.33}Co_{0.33}Mn_{0.33})O_2)$ is presented for NTC thermistor application. Thermogravimetric analysis-derivative thermogravimetry (TGA-DTG) identifies the optimal post-heat treatment temperature. The X-ray diffraction (XRD) patterns confirm a cubic spinel structure of the Ni-Co-Mn oxides, supported by scanning electron microscope (SEM) images showing a uniform microstructure. Also, energy dispersive X-ray spectroscopy (EDS) mapping confirms homogeneous element distribution. Recovered oxide pellets from the sintering process exhibit a single spinel structure, with X-ray photoelectron spectroscopy (XPS) analysis revealing changes in the valence states for Ni and Mn. Resistivity measurements demonstrate semiconductive behavior, which shows a B value (3376.92 K) suitable for NTC thermistor applications. This study contributes valuable insights to black powder recycling from EOL LIBs and its potential in temperature-sensitive electronic devices.

Keywords: temperature sensor; negative temperature coefficient; spinel; recycling

1. Introduction

Recent advancements in battery management systems (BMSs) require precise and accurate temperature monitoring within battery packs for battery safety and performance through efficient thermal management [1,2]. This can drive the development of temperature sensors with improved accuracy, response times, and stability over a wide temperature range. The negative temperature coefficient (NTC) thermistor is a type of temperature-sensitive resistor whose resistance decreases as the temperature increases, and they can be employed as temperature sensors for measuring the temperature of individual cells or modules within a battery pack [3–5]. Considering the temperature range over which the battery pack operates, the required accuracy, and environmental conditions, crystalline spinel oxides have been attractive as temperature sensors to exhibit the NTC of resistance due to their stable and predictable temperature resistance behavior. Among the spinel oxides, Ni-Mn-Co oxides have been extensively investigated to explore their electrical
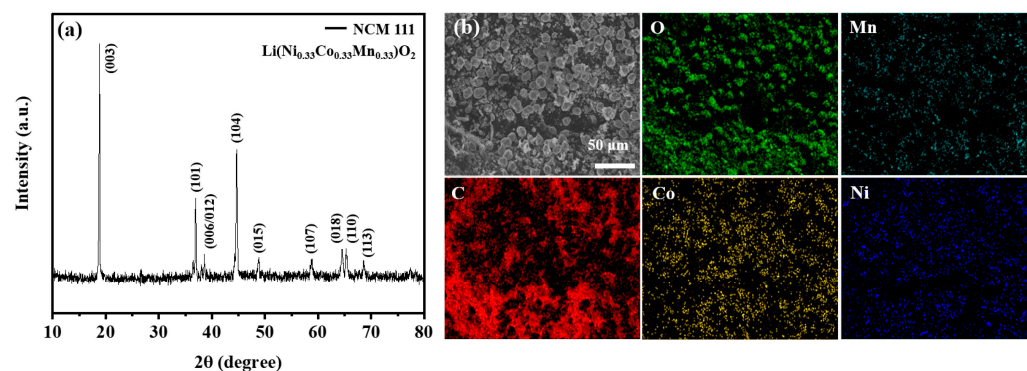
properties with temperature [4–10]. The spinel oxides can be prepared by combining various metal oxides (i.e., Co_3O_4, Mn_2O_3, and NiO) in precise ratios to tailor the temperature resistance behavior to match the specific needs of the battery pack. The NTC behavior of the spinel oxides is closely related to the presence of charge carriers (electrons or holes) and their mobility within the crystal lattice [4–8]. In other words, the mobility of charge carriers increases as the temperature increases, which leads to higher conductivity and thereby decreased resistance. Therefore, it is necessary to optimize the performance of NTC thermistors for their intended application in battery packs through tailoring the spinel oxides.

The rapid proliferation of lithium-ion batteries (LIBs) in diverse applications such as electric vehicles (EVs) and energy storage systems (ESSs) has led to a surge in demand and prices for key components in the cathodes of LIBs such as Li, Ni, Co and Mn [11–13]. The prevailing circumstances present a substantial challenge for manufacturing temperature sensors that rely on raw materials consisting of Ni-Co-Mn-based compounds, as it not only disrupts the smooth supply of raw materials but also contributes to an increase in manufacturing costs. To solve these challenges, there is ongoing development in the recycling technology of cathode materials used in LIBs using hydrometallurgy, pyrometallurgy, etc. [14]. Advancements in recycling technologies may lead to more efficient and cost-effective methods for recovering raw materials from an end-of-life (EOL) battery, which aims to offer a sustainable material supply while mitigating the rising prices of raw materials. This presents the potential to offer a sustainable resolution to the challenges connected with the growing demand and expenses of Ni, Co, and Mn, which serve as crucial components in industrial applications, including temperature sensors. However, very few reports are available in the literature investigating the spinel oxides using recycled materials from EOL batteries and its temperature-resistance behavior for the application of temperature sensors.

In this study, we develop the $(Ni_{0.6}Co_{0.4}Mn_2)O_4$ (NCM) spinel oxide via a solid state reaction using recycled Ni-Co-Mn oxides and investigate the electrical properties with temperature for the application of temperature sensors. Ni-Co-Mn oxide powder was prepared through precipitation of Ni-Co-Mn oxalate from black powder followed by post heat treatment. Material characterization of the recycled Ni-Co-Mn oxide powder were performed to show a crystalline spinel structure with a homogeneous elemental distribution. Also, the NCM showed NTC behavior, with a resistivity of 300 $\Omega\cdot$m and a B value of 3376.92 K, which are suitable for temperature sensors. This study highlights the potential for extracting rare metals and producing oxides from spent lithium-ion batteries, showcasing their applicability across various industrial sectors [15].

2. Results and Discussion

The XRD patterns of the black powder obtained from the EOL battery are presented in Figure 1a, which shows a well-defined hexagonal lattice of a layered α-$NaFeO_2$ structure with a space group of *R3m* (JCPDS#09-0063). Low peak intensities of carbon were also observed. The SEM images of the black powder show a particle size distribution of 1–10 μm with a spherical shape. In Figure 1b, the EDS mapping of the black powder reveals a homogeneous distribution of Mn, Co, Ni, and O with C. To obtain the information relating to the chemical composition of the structure in the black powder, ICP-OES analysis was performed to show the wt% of Ni, Co, and Mn as 15.8%, 16.8%, and 13.5%, respectively (Table 1). Based on the experimental results, the chemical composition of the black powder was $Li(Ni_{0.33}Co_{0.33}Mn_{0.33})O_2$ (NCM 111) with an *R3m* structure (JCPDS#09-0063), which is one of the typical cathode materials for lithium-ion batteries.
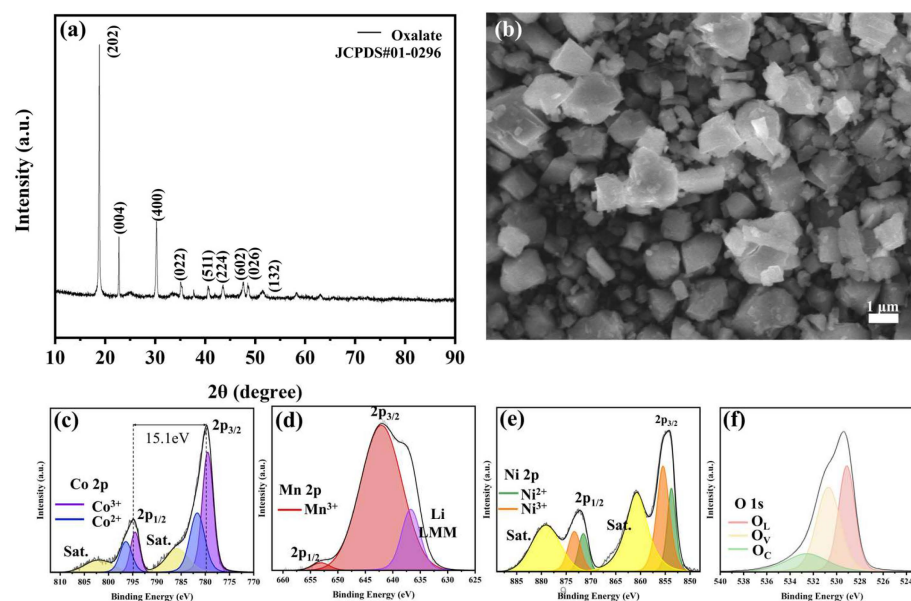
Figure 1. (**a**) XRD data of the black powder obtained from cathode of the end-of-life lithium-ion battery. (**b**) Micrographs of black powder and corresponding EDS mappings of different elements.

Table 1. Summary for ICP-OES data of Ni, Co, and Mn from black powder.

Sample No.	Unit	Ni	Mn	Co
1		15.8	16.8	13.5
2	wt%	15.5	16.2	13.2
3		15.7	16.7	13.4

The XRD patterns of the as-prepared sample via leaching of the black powder followed by a chemical reaction with oxalic acid is shown in Figure 2a, which presents a monoclinic structure with a $P2_1/m$ space group corresponding to a single oxalate phase (JCPDS#01-0296). Also, Figure 2b shows typical SEM images of the as-prepared sample, and the uniform micropolyhedron with 10 mm was the main product. The valence states of the cations (i.e., Ni, Co, and Mn) in the Ni-Mn-Co oxides were investigated using the XPS technique. The C 1s peak at 284.6 eV was set as the reference peak for calibrating all binding energies of the patterns. The Co 2p spectrum shows two major peaks near 779 eV and 795 eV (Figure 2c), which can be attributed to the Co $2p_{3/2}$ and Co $2p_{1/2}$ energy levels, since the spin orbit splitting for the Co 2p electron is approximately 15.1 eV [16]. Two satellite peaks corresponding to the Co $2p_{3/2}$ and Co $2p_{1/2}$ states were observed near 785 eV and 802 eV, respectively. It is noted that the Co 2p state of the Co^{3+} ions showed XPS signals of approximately 779.0 eV with a satellite peak at 785 eV, while the Co^{2+} ions in the metal oxides showed XPS signals of approximately 795 eV with a satellite peak at 802 eV [16–18]. Thus, the deconvoluted peaks of the Co 2p spectra can be assigned to the Co $2p_{3/2}$ and Co $2p_{1/2}$ energy levels, with their satellite peaks for the Co^{2+} cations in Ni-Mn-Co oxides. The XPS spectrum of the Mn 2p energy level shows two peaks at 637 eV and 642 eV for Mn $2p_{3/2,}$ and a satellite peak at 653 eV. The Mn 2p spectra was hampered by its overlapping with the Ni LMM Auger spectrum due to a low concentration of surface Mn [19]. However, when comparing the binding energies of the Mn 2p spectra for different Mn-based oxides, the deconvoluted peaks of the Mn 2p spectrum show the oxidation states of Mn^{3+} being located at the peak position at 642.1 eV and 636.7 eV (Figure 2d) [20]. Also, the Ni 2p spectrum shows two major peaks near 854 eV and 872.5 eV (Figure 2e), which can be attributed to the Ni $2p_{3/2}$ and Ni $2p_{1/2}$ energy levels. Also, satellite peaks at 861 eV and 879 eV were observed. Noted that the Ni 2p state of the Ni^{3+} ions showed XPS signals of approximately 855.5 eV and 873 eV, while the Ni^{2+} ions showed XPS signals of approximately 853 eV and 871 eV, indicating that the Ni had a mixed-valence state (i.e., Ni^{2+} and Ni^{3+}) [21–23]. The deconvoluted peaks of the O 1s spectrum were located at 529.1 eV, 530.7 eV, and 532.5 eV, corresponding to lattice oxygen, oxygen vacancy, and chemisorbed oxygen, respectively.
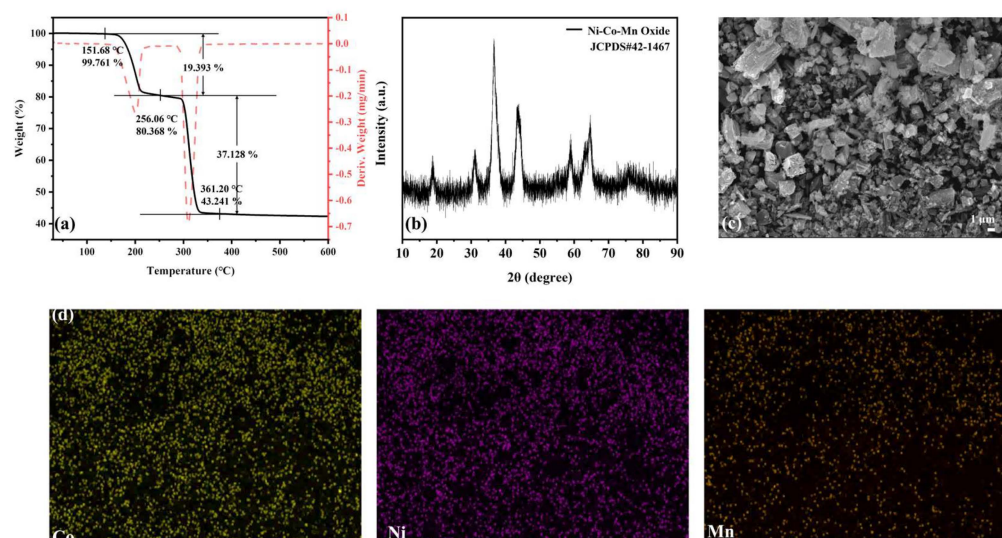
Figure 2. (**a**) XRD patterns and (**b**) micrographs of the Ni-Co-Mn oxalate powder after leaching process followed by chemical synthesis, as well as XPS analysis data of (**c**) Co 2p, (**d**) Mn 2p, (**e**) Ni 2p, and (**f**) O 1s.

To investigate the optimal temperature for transformation of the Ni-Mn-Co oxalate to oxides via post heat treatment, TGA-DTG was performed (Figure 3a). As the temperature increased above 151.68 °C, weight loss occurred, indicating H_2O loss. Also, another instance of abrupt weight loss was observed at approximately 305 °C. The TGA outcomes were in upright agreement with the DTG curve. Two observable peaks were noticed at 195 °C and 305 °C. In particular, the peak at 305 °C was related to the decomposition of oxalate ligand [24]. No further weight loss was observed in the 305–600 °C temperature range. The transformation of Ni-Mn-Co oxalates to Ni-Co-Mn oxides after post heat treatment in air was confirmed by the XRD patterns showing a cubic spinel structure. (JCPDS#42-1467) (Figure 3b). The weight percentage of Ni:Co:Mn was approximately 26.08%:21.31%:3.40%, which was confirmed by EDS analysis (Table 2). The morphology of the Ni-Co-Mn oxide powder was a uniform miropolyhedron with a size distribution of 1–10 μm (Figure 3c). Also, the EDS mapping confirmed the homogeneous distribution of Co, Mn, and Ni, which indicates that the Ni-Co-Mn oxide powder was successfully recovered from the black powder via the process in this study (Figure 3d).

Table 2. Quantitative EDS analysis of Ni-Co-Mn oxides.

Element	Wt%	At%
C	22.68	41.76
O	26.52	38.24
Mn	3.40	1.43
Co	21.31	8.34
Ni	26.08	10.25
Total	100	100

Figure 3. (**a**) TGA-DTG data, (**b**) XRD data, (**c**) micrograph, and (**d**) corresponding EDS mappings of the different elements of the oxide powder.

The XRD patterns of the sintered $(Ni_{0.6}Co_{0.4}Mn_2)O_4$ pellets prepared by a solid state reaction with the addition of the recovered Ni-Co-Mn oxides are shown in Figure 4a, indicating that the peak intensities at 18.0°, 30.0°, 35.4°, 37.0°, 43.0°, 53.3°, 56.8°, and 62.4° are matched well with (111), (022), (131), (222), (040), (242), (151), and (044) of the single spinel structure (JCPDS#42-1467), respectively. Also, the EDS mapping corresponding to the microstructure of the Ni-Co-Mn oxide pellets shows a homogeneous distribution of Ni, Mn, Co, and O (Figure 4b). The valence states of the cations (i.e., Ni, Co, and Mn) in the sintered pellet were evaluated using the XPS technique (Figure 5). The Co 2p spectrum showed two major peaks at 779.8 eV and 795.3 eV, corresponding to the Co $2p_{3/2}$ and Co $2p_{1/2}$ energy levels, respectively (Figure 5a). Two satellite peaks corresponding to the Co $2p_{3/2}$ and Co $2p_{1/2}$ states were observed at 785.8 eV and 801.8 eV, respectively. This indicates that the valence states of the Co were 2+ and 3+. The Ni 2p spectrum in Figure 5b shows XPS signals at 854.6 eV and 872.2 eV, with corresponding satellite peaks at 860.8 eV and 878.9 eV, respectively. This indicates that the valence state of Ni was 2+. Also, the XPS spectrum of the Mn 2p energy level showed two peaks at 641.3 eV and 653 eV, corresponding to Mn $2p_{3/2}$ and $2p_{1/2}$, respectively. The deconvoluted peaks of the Mn 2p spectrum showed different oxidation states, including Mn^{2+}, Mn^{3+}, and Mn^{4+} (Figure 5c). Also, the deconvoluted peaks of the O 1s spectrum were located at 529.5 eV, 530.6 eV, and 532.1 eV, corresponding to lattice oxygen, oxygen vacancy, and chemisorbed oxygen, respectively. Compared with the recovered Ni-Mn-Co oxide powder, the sintered pellet showed different valence states of Ni and Mn, and the oxidation states of Ni (2+ and 3+) were changed to 2+, while the oxidation states of Mn (2+ and 3+) changed to 2+, 3+, and 4+. The electric conduction of the $(Ni_{0.6}Co_{0.4}Mn_2)O_4$ pellet can be explained by the phonon-assisted hopping of charge carriers between the mixed transition elements with different valence states at the B sites (i.e., Mn^{3+}/Mn^{4+}) [25]. It is noted that heat treatment at a high temperature (>1050 °C) during sintering can lead to the reduction of Mn^{4+}/Mn^{3+} and the loss of excess oxygen, which can play an important role in electrical conduction of Ni-Co-Mn oxides with temperature [26].
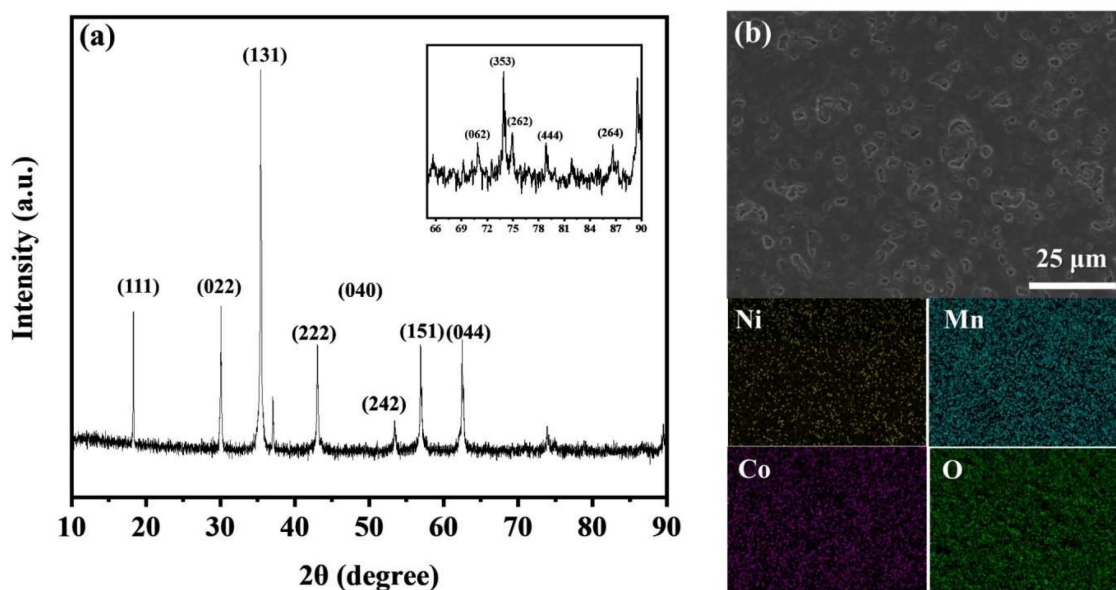
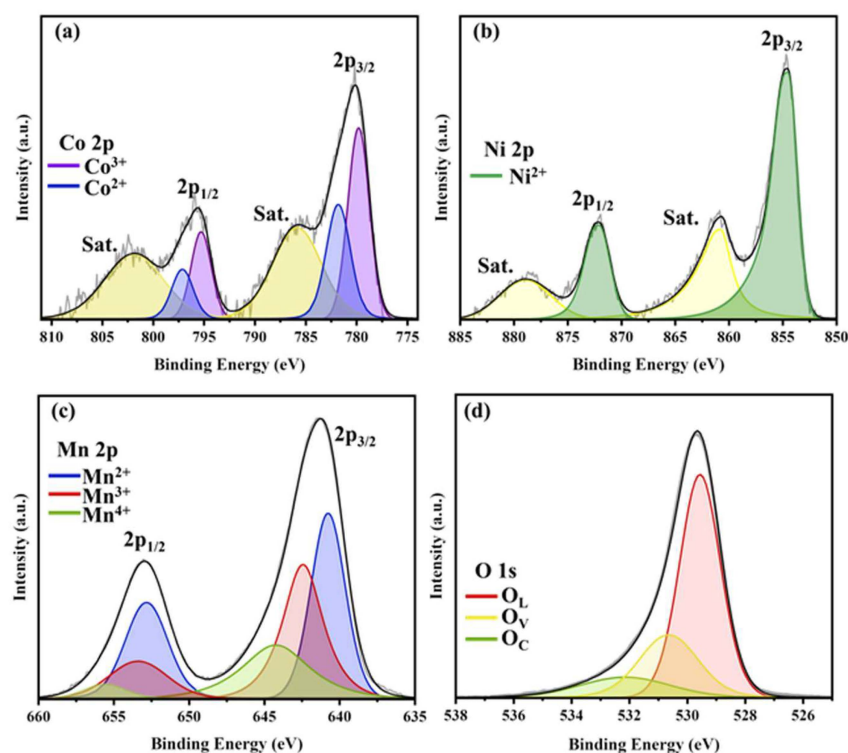**Figure 4.** (**a**) XRD data and (**b**) micrographs and corresponding EDS mapping of sintered Ni-Co-Mn oxides.

Figure 5. XPS analysis data of (**a**) Co 2p, (**b**) Ni 2p, (**c**) Mn 2p, and (**d**) O 1s of the sintered Ni-Co-Mn oxides.
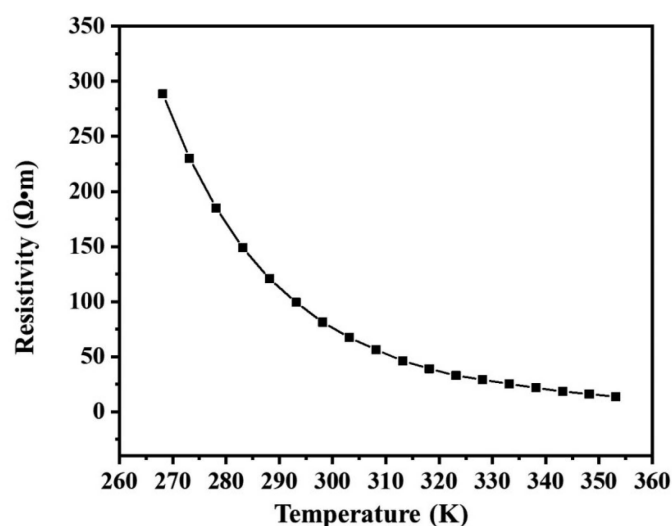
NTC thermistors are solid state temperature sensors that change their electrical resistance in response to temperature variations. To investigate the NTC properties of the $(Ni_{0.6}Co_{0.4}Mn_2)O_4$ pellet, the resistivity of the sintered pellet with temperature (268~353 K) was measured, and the results are shown in Figure 6. The sintered pellet showed semiconductive behavior, indicating decreased electrical resistivity with increased temperature [3].

The resistivity at 25 °C was approximately 300 Ω·m, and the B value was calculated to be 3376.92 K, as derived from Equations (1) and (2):

$$R = R_0 \exp\left(\frac{E_a}{k_b \cdot T}\right) = R_0 \exp\left(\frac{B}{T}\right) \tag{1}$$

$$B = \frac{T_1 \cdot T_2}{T_2 - T_1} \cdot \ln\left(\frac{R_1}{R_2}\right) \tag{2}$$

where B is the factor of thermal sensitivity, R is the resistance, k_B is the Boltzmann constant, and T is the absolute temperature. Note that the B value defines the relationship between the thermistor's resistance and temperature, which represents the material constant over a specific temperature interval (e.g., between T_1 and T_2) [27,28]. Also, a relationship between the resistance and temperature of the $(Ni_{0.6}Co_{0.4}Mn_2)O_4$ pellet can be utilized for temperature sensing applications. The typical B value range for an NTC thermistor may vary depending on the intended industrial application. However, a commonly observed range for the B value of such NTC thermistors is typically from 3000 K to 5000 K. The NTC thermistor, prepared using recycled Ni-Co-Mn oxides in this study, demonstrates its potential for industrial applications through the recycling of cathode materials from EOL LIBs. This potential is evident due to its compatibility with the commonly observed B value range.

Figure 6. Resistivity of the sintered Ni-Co-Mn oxides in the temperature range between 268 K and 353 K.

3. Experimental Procedures

We employed a wet processing method to prepare Ni-Co-Mn oxalates, utilizing black powder composed of $Li(Ni_{0.33}Co_{0.33}Mn_{0.33})O_2$, which was obtained from quantitative analysis using inductively coupled plasma with optical emission spectrometry (ICP-OES, iCAP 7000, Thermo Fisher Scientific, USA) after the black powder was dissolved. For optimal recovery of Ni, Co, and Mn, a solution-to-black-powder ratio of 1:20 (pulp density 20 g/L) was maintained during leaching. The process involved placing 7 g of black powder into a round-bottomed flask. A mixed solution (350 mL) of 1 M H_2SO_4 and 0.075 M $NaHSO_4$ at a 1:1 ratio with D.I. water was added to the flask. The mixed solution was stirred at 90 °C for 4.5 h. To prevent the evaporation of H_2O from the flask, it was completely sealed, and the temperature was monitored using a temperature sensor. After stirring, filtration was performed to separate the leachate and leaching solution. Then, 1 M of oxalic acid was added to a round-bottomed flask with the leaching solution. The solution was stirred at 50 °C for 16 h, and precipitation was separated from the solution, followed by washing three times and drying at 90 °C for 24 h for preparation of the cobalt oxalate. The obtained

Ni-Co-Mn oxalates were heat-treated at 450 °C for 3 h with a heating rate of 3.75 °C/min for the preparation of Ni-Co-Mn oxides ($(Ni_{1.54}Co_{1.25}Mn_{0.21})O_4$). The recovered powder was mixed with Mn_3O_4 and NiO powers to prepare $(Ni_{0.6}Co_{0.4}Mn_2)O_4$ via a solid state reaction ($(Mn_3O_4: Ni_{1.54}Co_{1.25}Mn_{0.21})O_4: NiO = 1.8:0.9:0.3)$).

The powders were added into the beaker with ethanol, and the mixture was stirred for 3 h. Then, the mixture was dried at 90 °C for over 12 h. The powders were pressed into pellets using a pressure (Pellet press TN, LPP-25T, Puchong, Malaysia) of 20 MPa to prepare 1.25 mm-thick and 25 mm-in-diameter pellets. The green compacts were sintered at 1250 °C for 8 h and then cooled to 900 °C for 2 h before cooling to 25 °C. The crystallographic information and microstructure of the black powder recovered Ni-Co-Mn oxide powder, and NCM pellets were observed using an X-ray diffractometer (XRD, Empyrean, Malvern Panalytical, UK) with Cu Kα radiation (λ = 1.5404 Å) and scanning electron microscopy (SEM, JSM-7610F PLUS, JEOL, Japan), respectively. Additionally, the element distribution of the samples was analyzed using energy dispersive X-ray spectroscopy (EDS-7557, Oxford Instruments, UK). The oxidation states of the elements in the samples were measured using an X-ray photoelectron spectrometer (XPS, NEXSA, ThermoFisher Scientific, USA). Also, Thermogravimetric analysis-derivative thermogravimetry (TGA-DTG, TGA 8000, Perkin Elmer, USA) was performed to investigate the crystallization behavior of the Ni-Co-Mn oxalates. To evaluate the B value for application to temperature sensors, the electrical resistance was measured in the temperature range between 268 K and 353 K using an LCR meter (IM3570, Hioki, Japan) after applying the silver paste on the surface of the pellets.

4. Conclusions

A systematic investigation into the synthesis and characterization of recovered Ni-Co-Mn oxides obtained from black powder of the cathode materials ($Li(Ni_{0.33}Co_{0.33}Mn_{0.33})O_2$) of EOL LIBs has been presented for the application of NTC thermistors. The leaching of the black powder, followed by a chemical reaction with oxalic acid, led to the formation of a monoclinic structure corresponding to a single oxalate phase. The XPS analysis provided insights into the valence states of the cations (Ni, Co, and Mn) in the Ni-Mn-Co oxides. Moreover, TGA-DTG analysis elucidated the optimal temperature for the transformation of Ni-Mn-Co oxalates into Ni-Mn-Co oxide powder during post heat treatment. The recovered Ni-Co-Mn oxides were confirmed through XRD patterns displaying a cubic spinel structure, accompanied by SEM images showing a uniform micropolyhedron morphology (1–10 μm). EDS mapping confirmed the homogeneous distribution of Co, Mn, and Ni in the recovered oxides. The recovered Ni-Co-Mn oxide pellets prepared by a solid-state reaction exhibited a single spinel structure. XPS analysis of the sintered pellet revealed changes in the valence states for Ni and Mn compared with the recovered Ni-Mn-Co oxides, which plays an important role in electrical conduction with temperature. The resistivity measurements demonstrated semiconductive behavior with decreasing electrical resistivity as the temperature increased. The calculated B value, indicative of the temperature coefficient of resistance, placed the Ni-Mn-Co oxide pellet at 3376.92 K, making it suitable for NTC thermistor applications. The comprehensive findings presented in this study contribute valuable insights in the field of recycling of black powder obtained from end-of-life lithium-ion batteries and have potential applications in temperature-sensitive electronic devices.

Data Availability Statement: The raw data supporting the conclusions of this article will be made available by the author on request.

Conflicts of Interest: The author declares no conflict of interest.

References

1. Chan, C.C.; Chau, K.T. An overview of power electronics in electric vehicles. *IEEE Trans. Ind. Electron.* **1997**, *44*, 3–13. [CrossRef]
2. Zahid, T.; Li, W.M. A comparative study based on the least square parameter identification method for state of charge estimation of a LiFePO$_4$ battery pack using three model-based algorithms for electric vehicles. *Energies* **2016**, *9*, 720. [CrossRef]
3. Han, H.; Lee, J.S.; Ryu, J.H.; Kim, K.M.; Jones, J.L.; Lim, J.; Guillemet-Fritsch, S.; Lee, H.C.; Mhin, S. Effect of high cobalt concentration on hopping motion in cobalt manganese spinel oxide (Co$_x$Mn$_{3-x}$O$_4$, x $\geq$ 2.3). *J. Phys. Chem. C* **2016**, *120*, 13667–13674. [CrossRef]
4. Bhargava, A.; Eppstein, R.; Sun, J.; Smeaton, M.A.; Paik, H.; Kourkoutis, L.F.; Schlom, D.G.; Toroker, M.C.; Robinson, R.D. Breakdown of the small-polaron hopping model in higher-order spinels. *Adv. Mater.* **2020**, *32*, 2004490. [CrossRef] [PubMed]
5. Zhang, H.M.; Chang, A.M.; Peng, C.W. Preparation and characterization of Fe^{3+}-doped Ni$_{0.9}$Co$_{0.8}$Mn$_{1.3-x}$Fe$_x$O$_4$ (0 <= x <= 0.7) negative temperature coefficient ceramic materials. *Microelectron. Eng.* **2011**, *88*, 2934–2940.
6. Muralidharan, M.N.; Sunny, E.K.; Dayas, K.R.; Seema, A.; Resmi, K.R. Optimization of process parameters for the production of Ni-Mn-Co-Fe based NTC chip thermistors through tape casting route. *J. Alloys Compd.* **2011**, *509*, 9363–9371. [CrossRef]
7. Han, H.; Mhin, S.; Park, K.R.; Kim, K.M.; Lee, J.I.; Ryu, J.H. Fe doped Ni-Mn-Co-O ceramics with varying Fe content as negative temperature coefficient sensors. *Ceram. Int.* **2017**, *43*, 10528–10532. [CrossRef]
8. Yokoyama, T.; Meguro, T.; Nakamura, M.; Tatami, J.; Wakihara, T.; Komeya, K. Fabrication and electrical properties of sintered bodies composed of Mn$_{(1.75-1.25X)}$Co$_{2.5X}$Ni$_{1.25(1-X)}$O$_4$ (0 $\leq$ X $\leq$ 0.6) with a cubic spinel structure. *J. Ceram. Process. Res.* **2009**, *10*, 683–688.
9. Teichmann, C.; Töpfer, J. Sintering and electrical properties of Cu-substituted Zn-Co-Ni-Mn spinel ceramics for NTC thermistors thick films. *J. Eur. Ceram. Soc.* **2022**, *42*, 2261–2267. [CrossRef]
10. Li, H.; Ley Thayil, I.P.; Ma, X.; Sang, X.; Zhang, H.; Chang, A. Electrical properties and aging behavior of Na-doped Mn$_{1.95}$Co$_{0.21}$Ni$_{0.84}$O$_4$ NTC ceramics. *Ceram. Int.* **2020**, *46*, 24365–24370. [CrossRef]
11. Li, L.; Zhang, X.; Li, M.; Chen, R.; Wu, F.; Amine, K.; Lu, J. The Recycling of Spent Lithium-Ion Batteries: A Review of Current Processes and Technologies. *Electrochem. Energy Rev.* **2018**, *1*, 461–482. [CrossRef]
12. Liu, Y.; Hou, Y.; Liu, L.; Chen, J.; Wang, J. Nanostructured carbon-based cathode materials for non-aqueous Li-O$_2$ batteries. *Mater. Lab.* **2023**, *2*, 220015.
13. Li, H.; Chen, J.; Fang, J. Recent Advances in Wearable Aqueous Metal-Air Batteries: From Configuration Design to Materials Fabrication. *Adv. Mater. Technol.* **2023**, *8*, 2201762. [CrossRef]
14. Baum, Z.J.; Bird, R.E.; Yu, X.; Ma, J. Lithium-Ion Battery Recycling—Overview of Techniques and Trends. *ACS Energy Lett.* **2022**, *7*, 712–719. [CrossRef]
15. Wei, J.; Zhao, S.; Ji, L.; Zhou, T.; Miao, Y.; Scott, K.; Li, D.; Yang, J.; Wu, X. Reuse of Ni-Co-Mn oxides from spent Li-ion batteries to prepare bifunctional air electrodes. *Resour. Conserv. Recycl.* **2018**, *129*, 135–142. [CrossRef]
16. Fu, C.C.; Li, G.S.; Luo, D.; Huang, X.S.; Zheng, J.; Li, L.P. One-step calcination-free synthesis of multicomponent spinel assembled microspheres for high-performance anodes of Li-Ion batteries: A case study of MnCo$_2$O$_4$. *ACS Appl. Mater. Interfaces* **2014**, *6*, 2439–2449. [CrossRef]
17. Wakisaka, Y.; Hirata, S.; Mizokawa, T.; Suzuki, Y.; Miyazaki, Y.; Kajitani, T. Electronic structure of Ca$_3$Co$_4$O$_9$ studied by photoemission spectroscopy: Phase separation and charge localization. *Phys. Rev. B* **2008**, *78*, 235107. [CrossRef]
18. Munakata, F.; Takahashi, H.; Akimune, Y.; Shichi, Y.; Tanimura, M.; Inoue, Y.; Itti, R.; Koyama, Y. Electronic state and valence control of LaCoO$_3$: Difference between La-deficient and Sr-substituting effects. *Phys. Rev. B* **1997**, *56*, 979–982. [CrossRef]
19. Zhu, J.; Zheng, J.; Cao, G.; Li, Y.; Zhou, Y.; Deng, S.; Hai, C. Flux-free synthesis of single-crystal LiNi$_{0.8}$Co$_{0.1}$Mn$_{0.1}$O$_2$ boosts its electrochemical performance in lithium batteries. *J. Power Sources* **2007**, *174*, 965–969. [CrossRef]
20. Ni, L.; Guo, R.; Deng, W.; Wang, B.; Chen, J.; Mei, Y.; Gao, J.; Gao, X.; Yin, S.; Liu, H.; et al. Single-Crystalline Ni-Rich layered cathodes with Super-Stable cycling. *Chem. Eng. J.* **2022**, *431*, 133731. [CrossRef]
21. Chen, Y.; Liu, Y.; Zhai, W.; Liu, H.; Sakthivel, T.; Guo, S.; Dai, Z. Metastabilizing the Ruthenium Clusters by Interfacial Oxygen Vacancies for Boosted Water Splitting Electrocatalysis. *Adv. Energy Mater.* **2024**, *14*, 2400059. [CrossRef]
22. Zhai, W.; Chen, Y.; Liu, Y.; Sakthivel, T.; Ma, Y.; Qin, Y.; Qu, Y.; Dai, Z. Enlarging the Ni–O Bond Polarizability in a Phosphorene-Hosted Metal–Organic Framework for Boosted Water Oxidation Electrocatalysis. *ACS Nano* **2023**, *17*, 17254–17264. [CrossRef] [PubMed]
23. Zhai, W.; Chen, Y.; Liu, Y.; Ma, Y.; Vijayakumar, P.; Qin, Y.; Qu, Y.; Dai, Z. Covalently Bonded Ni Sites in Black Phosphorene with Electron Redistribution for Efficient Metal-Lightweighted Water Electrolysis. *Nano-Micro. Lett.* **2024**, *16*, 115. [CrossRef] [PubMed]
24. Ghosh, S.; Jana, R.; Ganguli, S.; Inta, H.R.; Tudu, G.; Koppisetti, H.V.S.R.M.; Datta, A.; Mahalingam, V. Nickel–cobalt oxalate as an efficient non-precious electrocatalyst for an improved alkaline oxygen evolution reaction. *Nanoscale Adv.* **2021**, *3*, 3770–3779. [CrossRef]
25. Muralidharan, M.; Rohini, P.; Sunny, E.K.; Dayas, K.R.; Seema, A. Effect of Cu and Fe addition on electrical properties of Ni–Mn–Co–O NTC thermistor compositions. *Ceram. Int.* **2012**, *38*, 6481–6486. [CrossRef]
26. Jeon, J.; Park, K.R.; Kim, K.M.; Ahn, C.; Lee, J.; Yu, D.; Bang, J.; Oh, N.; Han, H.; Mhin, S. Effect of Cu/Fe addition on the microstructures and electrical performances of Ni–Co–Mn oxides. *J. Alloys Compd.* **2021**, *859*, 157769. [CrossRef]

27. Gao, C.; Li, Z.; Yang, L.; Peng, D.; Zhang, H. Investigation of electrical and aging properties of Bi-modified $(Zn_{0.4}Ni_{0.6})_{1-x}Na_xO$ ceramic thermistors. *J. Eur. Ceram. Soc.* **2021**, *41*, 4160–4166. [CrossRef]

28. Hardian, A.; Greshela, S.; Yuliana, T.; Budiman, S.; Murniati, A.; Kusumaningtyas, V.A.; Syarif, D.G. Cu-Mn Co-doped $NiFe_2O_4$ based thick ceramic film as negative temperature coefficient thermistors. *Earth Environ. Sci.* **2021**, *882*, 012017. [CrossRef]